Senior Honors Projects   Honor's Program

2021

Analyzing the Optical Properties of Hemozoin to Expand the Disease Detection Applications of a Magneto-Optical Device (MOD)

Kyle Blasinsky

Analyzing the Optical Properties of Hemozoin
to Expand the Disease Detection Applications
of a Magneto-Optical Device (MOD)

Kyle J. Blasinsky[1, a)], Jessica Thomas[1], Amanda McGreer[1],
Robert Deissler[2], Robert Brown[2], Danielle Kara[1]

[1] *John Carroll University, 1 John Carroll Boulevard, University Heights, OH 44118*
[2] *Case Western Reserve University, 10900 Euclid Avenue, Cleveland, OH 44106*

[a)] Corresponding author: kblasinsky20@jcu.edu

Abstract. Hemozoin crystals are the basis of a new approach for efficient, cost-effective malaria detection. Clinical success of malaria detection with a magneto-optical device (MOD) motivates quantification of the optical interactions forming the basis of the detection mechanism. The MOD is used to measure the intensity of polarized light transmitted through a sample of hemozoin suspended in phosphate-buffered saline, subject to a magnetic field, $\vec{B}$, that can be turned on and off. According to Beer's law, ratios of transmitted light with different polarization directions and with $\vec{B}$ on and off as a function of hemozoin concentration were related to change in absorption cross section, $\Delta\sigma$, an important property for quantifying optical interactions. Using two methods, $\Delta\sigma$ was uniquely determined, producing similar results, supporting the physical and mathematical theory used to understand MOD's detection mechanism. Successful quantification of $\Delta\sigma$ informs our understanding of the magneto-optical properties of hemozoin, which advances malaria detection, and expands potential applications of the MOD.

INTRODUCTION

In 2018, 228 million cases of malaria were reported worldwide, leading to roughly 405,000 deaths. Additionally, 2.7 billion dollars was spent on prevention and elimination programs in 2018, coupling financial costs with already significant human costs.[1] Malaria is still highly prevalent in the international community, particularly in the developing world. The disease is especially prolific in African, southeast Asian, and central and south American nations, many of which are still developing.[1] Given the levels of medical infrastructure in these nations, where over 3.4 billion people live at-risk of developing malaria, traditional diagnostic mechanisms are not financially or structurally feasible. A simpler, faster, and more affordable novel approach of detecting malaria is needed.[2]

Pathologists tend to be few and far between in at-risk nations and with over a billion tests needed per year, expensive and time-consuming diagnostic tests cannot effectively meet the needs of the world's most vulnerable communities. However, malaria parasites produce a physically interesting and a diagnostically invaluable byproduct, a pigment known as hemozoin. Hemozoin is produced by all variants of malaria parasites while they consume hemoglobin in a host's blood.[3,4] Medical technologies can exploit physical characteristics of hemozoin crystals to

detect malaria. The human body on its own will never produce hemozoin, so if hemozoin is detected in a blood sample, it must be coming from a malaria parasite.[5]

Hemozoin molecules have a top like shape with a porphyrin ring of carbon and nitrogen atoms surrounding a central iron atom. A single oxygen atom protrudes from this planar ring of carbon and iron as seen in Figure 1a.[6] Individual molecules stack to form the long, thin, rod-shaped crystals seen in Figures 1b and 1c. The long axis of these crystals measures roughly 700 nanometers and is referred to as the hard axis. The short axes of the crystals are considerably shorter in length and together defined a plane referred to as the easy plane.[6]

Figure 1a.

b.

c.
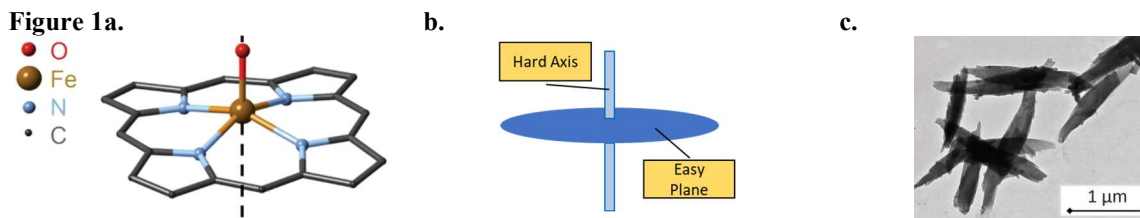
a) A single molecule of hemozoin with an outer planar region of carbon (C) known as a porphyrin ring surrounding four nitrogen atoms (N), together spatially referend to as falling within the easy plane. The central iron (Fe) atom contributes to hemozoin's unique magnetic properties and, along with the oxygen (O) atom, falls along hemozoin's hard axis depicted by the dashed, vertical line. From Butykai, et al. b) A simplified geometric representation of a hemozoin crystal. The crystal has two distinct geometric features, a planar region referred to as the easy plane, and a long, central axis referred to as the hard axis. The easy plane is defined by the short axes of the crystal and contains molecules' porphyrin ring of carbon and nitrogen. The hard axis is defined by the long axis of the crystal and contains molecules' central, iron-oxygen axis. c) Transmission electron micrograph of hemozoin crystals displaying the pigment's rod-like structure. From Butykai, et al.

The geometry and chemical composition of hemozoin gives rise to two properties that make the crystal ideal for detection with MOD. The first is magnetic anisotropy. The central iron atom in hemozoin molecules makes its magnetic moment stronger in the easy plane of each molecule than along the hard axis.[6] The second diagnostically invaluable characteristic of hemozoin is the dichroism that the crystals exhibit. Dichroism is a directionally dependent efficiency at absorbing light.[7] Because hemozoin's porphyrin ring allows electrons to move more freely within the ring than they would along the hard axis, light polarized parallel to the easy plane allows for maximum optical interactions between the incident light and the crystals, leading to minimal transmission. Conversely, light polarized parallel to the hard axis has minimal optical interactions with the crystals, allowing for maximum transmission.

MOD uses both of these characteristics of the crystals to detect hemozoin. Because the light used in the MOD can be polarized in different directions, hemozoin samples can be tested in the MOD to see how optical interactions with the crystals are affected by the application of a magnetic field. The direction of this magnetic field is fixed, but the magnets producing the field can be moved on and off the sample. When hemozoin is present and the magnetic field is applied, the crystals, free to move in solution, rotate, aligning their easy plane with the magnetic field.[6] If the polarization direction of light is parallel to the magnetic field, minimal transmission occurs. Maximum transmission

occurs when polarization direction is perpendicular to the magnetic field. Without hemozoin present though, the transmitted light intensity is unaffected by application of the magnetic field.

The diagnostic mechanism MOD utilizes to detect malaria via hemozoin works extremely well and can be utilized in the detection of other diseases as well. Other crystals associated with various diseases, including gout and pseudo gout, exhibit properties similar to hemozoin and can be detected using the MOD.[8] Other diseases may even be detectable using magnetic nanoparticles rather than physically unique crystals. However, expanding the applications of MOD is contingent on a sound physical understanding of the optical interactions underlying the existing hemozoin detection mechanism.

Quantification of hemozoin's optical properties informs our understanding of the MOD detection mechanism, which advances malaria detection and ultimately broadens MOD's detection capabilities. Absorption cross section, σ, was sought as a means of quantifying these properties. Utilizing Beer's law and Euler angles for a basis transformation, two methods for determining the difference in absorption cross section for light polarized along hemozoin's principal axes were developed, tested, and compared. Agreement of these results provides assurance that the theory underlying quantification is sound, paving the way to utilize MOD with other crystals and particles for the detection of additional diseases.

THEORY

In order to demonstrate an understanding of the physical interaction between light and hemozoin, methods must be derived to quantify the interaction. Absorption cross section, σ, was utilized as it measures the effective area of a material that photons need to interact with in order to be absorbed.[9] Given the dichroism exhibited by hemozoin molecules, it is important to understand the relative difference in σ along each of the crystal's three principal axes.

Figure 2a.   **b.**
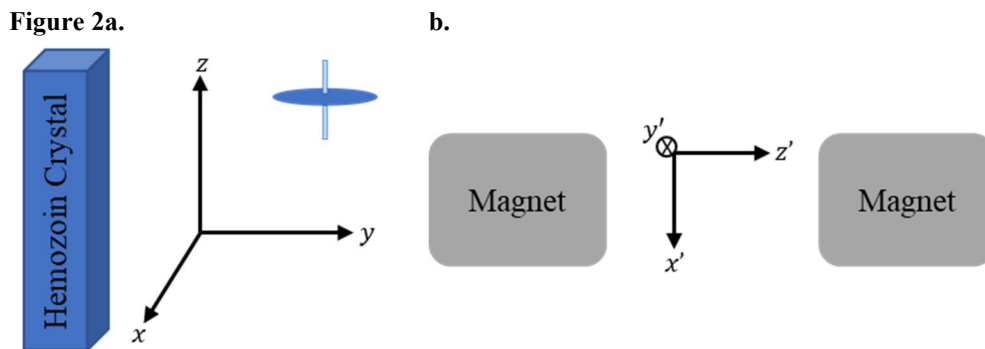
a) A representation of a hemozoin crystal (left) relative to the unprimed, crystal coordinate system. A copy of Fig. 1b is added (right) to relate this coordinate system to the easy plane and hard axis. b) Two magnets aligned, as they are in the MOD, to produce an external magnetic field between them relative to the primed, laboratory coordinate system.

3

Given the symmetry of hemozoin crystals, as depicted in Fig. 2a, σ_x and σ_y, the absorption cross section along the x and y axes respectively, are presumed equal. Therefore, $\Delta\sigma$ as in Eq. (1) is sought.

$$\Delta\sigma = \sigma_x - \sigma_z \tag{1}$$

Beer's law seen in Eq. (2), where I_0 is incident light intensity, I is transmitted light intensity, ℓ is path length (cm), and N is sample concentration ($crsyals/cm^3$), contains an absorption cross section term. The exponential term that contains σ is not ideal though. However, given that $\sigma\ell N \ll 1$, Eq. (2) can be roughly equated to Eq. (3), an approximate linear form of Beer's law derived using a first-order Taylor series approximation.

$$\frac{I}{I_0} = e^{-\sigma\ell N} \tag{2}$$

$$\frac{I}{I_0} \cong 1 - \sigma\ell N \tag{3}$$

Intensity data collected in the primed laboratory frame of reference must be averaged over many crystal orientations caused by thermal fluctuations and converted into the unprimed crystal frame of reference to produce a measure of a hemozoin crystals' absorption cross section. Using Euler angles to complete the basis transformation and averaging over thermal fluctuations, the relations for absorption cross sections in each reference frame can be related for different polarization directions while the magnetic field is applied, $\sigma_{x'B}$ and $\sigma_{z'B}$, and without the magnetic field applied, $\sigma_{No\,B}$ (see appendix).

Assuming strong magnetic field.

$$\langle\sigma_{x'B}\rangle = \frac{1}{2}\sigma_x + \frac{1}{2}\sigma_z \tag{4}$$

$$\langle\sigma_{z'B}\rangle = \sigma_x \tag{5}$$

$$\langle\sigma_{No\,B}\rangle = \frac{2}{3}\sigma_x + \frac{1}{3}\sigma_z \tag{6}$$

With the coordinate systems related, the first method for determining $\Delta\sigma$ can be undertaken. Method 1 compares intensity ratios as functions of N.

$$\frac{I_{x'B}}{I_{x'No\,B}} \cong 1 - N\ell(\langle\sigma_{x'B}\rangle - \langle\sigma_{x'No\,B}\rangle) \tag{7}$$

$$\frac{I_{z'B}}{I_{z'No\,B}} \cong 1 - N\ell(\langle\sigma_{z'B}\rangle - \langle\sigma_{z'No\,B}\rangle) \tag{8}$$

$$\frac{I_{x'B}}{I_{z'B}} \cong 1 - N\ell(\langle\sigma_{x'B}\rangle - \langle\sigma_{z'B}\rangle) \tag{9}$$

Because these absorption cross sections correspond to the laboratory frame of reference, each can be converted to the crystal frame of reference by plugging Eqs. (4), (5), and (6) into Eqs. (7), (8), and (9).

$$\frac{I_{x'B}}{I_{x'No\ B}} \cong 1 - N\ell \left[\frac{-1}{6}(\sigma_x - \sigma_z)\right] \tag{10}$$

$$\frac{I_{z'B}}{I_{z'No\ B}} \cong 1 - N\ell \left[\frac{1}{3}(\sigma_x - \sigma_z)\right] \tag{11}$$

$$\frac{I_{x'B}}{I_{z'\ B}} \cong 1 - N\ell \left[\frac{-1}{2}(\sigma_x - \sigma_z)\right] \tag{12}$$

Method 2 compares intensity ratios as multiples of a base concentration. If β is the base concentration and m is a constant of proportionality, then N can be redefined as in Eq. (13).

$$N = m\beta \tag{13}$$

Eq. (13) can be used to derive a new set of Beer's law equations.

$$\frac{I_{m,x'}}{I_{\beta,x'}} \cong 1 - \beta(m-1)\ell\langle\sigma_{x'}\rangle \tag{14}$$

$$\frac{I_{m,z'}}{I_{\beta,z'}} \cong 1 - \beta(m-1)\ell\langle\sigma_{z'}\rangle \tag{15}$$

$$\frac{I_{m,No\ B}}{I_{\beta,No\ B}} \cong 1 - \beta(m-1)\ell\langle\sigma_{x'No\ B}\rangle = 1 - \beta(m-1)\ell\langle\sigma_{z'No\ B}\rangle \tag{16}$$

Again, because these absorption cross sections correspond to the laboratory frame of reference, each can be converted to the crystal frame of reference by plugging Eqs. (4), (5), and (6) into Eqs. (14), (15), and (16).

$$\frac{I_{m,x'}}{I_{\beta,x'}} \cong 1 - \beta(m-1)\ell\left(\frac{1}{2}\sigma_x + \frac{1}{2}\sigma_z\right) \tag{17}$$

$$\frac{I_{m,z'}}{I_{\beta,z'}} \cong 1 - \beta(m-1)\ell\sigma_x \tag{18}$$

$$\frac{I_{m,x'No\ B}}{I_{\beta,x'No\ B}} = \frac{I_{m,z'No\ B}}{I_{\beta,z'No\ B}} \cong 1 - \beta(m-1)\ell\left(\frac{2}{3}\sigma_x + \frac{1}{3}\sigma_z\right) \tag{19}$$

METHODS

In 2017, United States Patent No. 9,778,245-B2 was issued to researchers from Case Western Reserve University for a diagnostic device that used light and magnets to detect hemozoin in blood samples and ultimately detect malaria.[10] The device depicted in Fig. 3a is a finalized model of an apparatus that came to be licensed by Hemex Health for rapid, cost-effective, and highly accurate detection of malaria.[2] The device depicted in Fig. 3b is an earlier

iteration of the device granted the patent and licensed to Hemex Health. This prototype was provided to the Kara Lab at John Carroll University by researchers at Case Western Reserve University, to whom the aforementioned patent was issued, for use in this research.

Figure 3a.
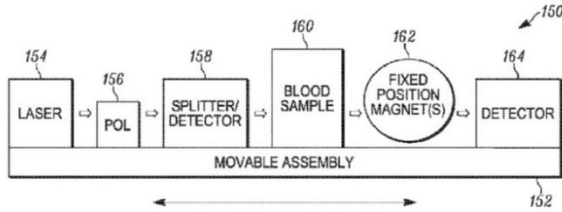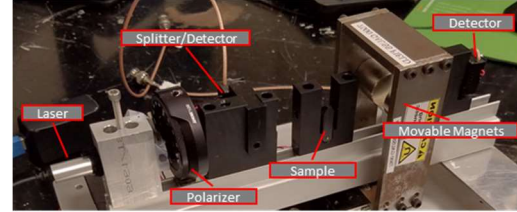
a) A diagram from United States Patent No. 9,778,245-B2 depicting the major components of the apparatus that has demonstrated success of hemozoin and, subsequently, malaria detection. b) A photo from the Kara Lab of the prototype of the final model shown in Fig. 3a used in this research. The major components of the device are labeled similar to the device in Fig. 3a to highlight similarities between the two apparatuses.

The complete MOD set-up has three major components, a source of polarized light, control and transmission photodetectors, and two strong moveable magnets. To produce the source of polarized light, a monochromatic laser sent light through a linear polarizer before the then polarized light entered a beam-splitter. The splitter created two roughly equal intensity beams; one beam entered the control photo detector while the other continued to the sample. Whatever component of the beam was transmitted through the sample entered the second photodetector. Both photodetectors' output voltages were automatically input into LabView with a data acquisition tool.

Figure 4.
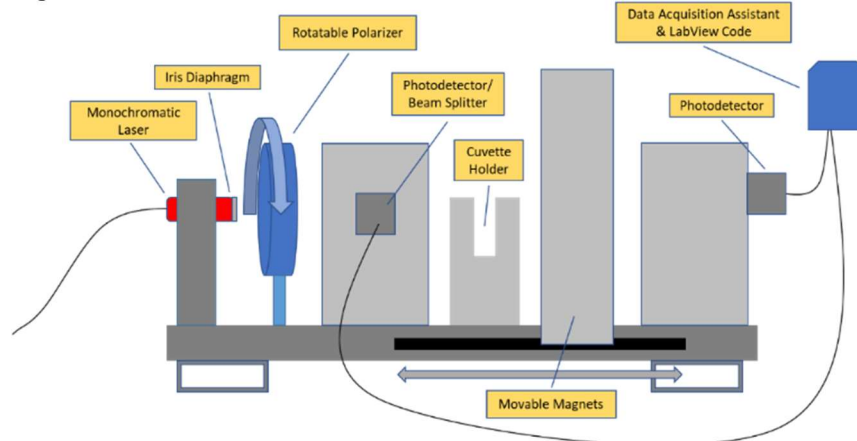
A diagram of the MOD prototype used for data collection. From left to right, there is a monochromatic laser attached to an iris diaphragm that controlled the beam's shape. Next is a rotatable linear polarizer that allowed the polarization direction to be alternated between the x' and y' directions. Following is the beam splitter and the first photodetector (control) which was monitored to ensure the laser's output was steady. Immediately right is the cuvette holder where samples were housed during trials. This holder is next to the apparatus' strong magnets which could be slid along a track so that the magnets could be moved directly next to the sample housing. Beyond the magnets is the final photodetector (transmission) which is connected to a data acquisition tool and LabView, as is the control photodetector.

6

To collect data, samples were produced at several concentrations ranging from 0.5ng/µL to 20ng/µL by combining dry Invivogen hemozoin with phosphate-buffered saline (PBS). These solutions were sonicated to evenly distribute the hemozoin crystals and randomize their orientation before each trial. Intensity was measured with no sample, with no magnetic field applied, and with a magnetic field applied. Data was collected in LabView and subsequently analyzed in Excel.

Figure 5.

Hemozoin at 20ng/µL with horizontally polarized incident light
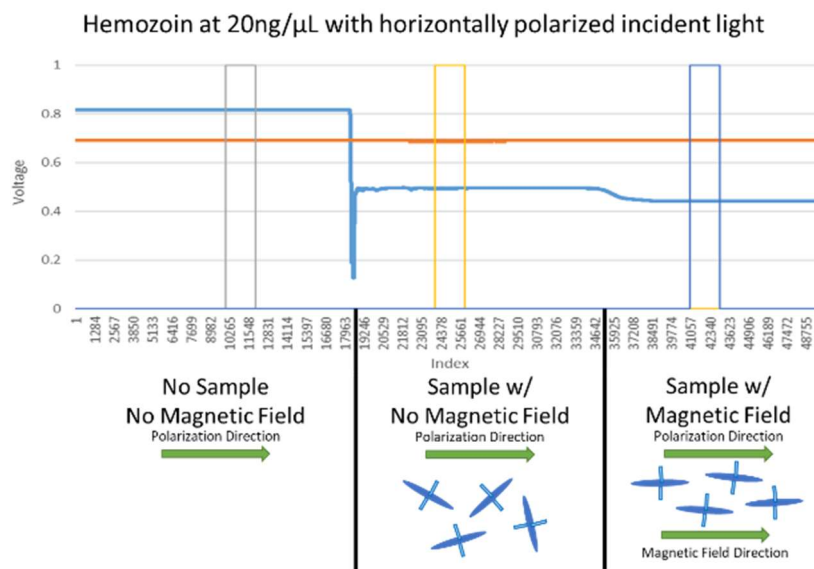
Displayed is a graph of the output voltages from each photodetector as a function of a generic index representing time. The steady orange line shows the output from the control photodetector and the changing blue line shows the output from the transmission photodetector. There are three distinct regions present in the transmission detector's output, the first showing when no sample and no magnetic field are present, the second showing when the sample is in the MOD but the magnetic field has not yet been applied (here the hemozoin crystals orient themselves totally randomly), and the third showing when the sample is present and the magnetic field is applied (here the hemozoin crystals rotate so that their easy plane is parallel to the magnetic field). The grey, yellow, and blue rectangles were used to visually show which data points were averaged to find an intensity value for each region during data analysis. In this display, there is a drop from the second to third region, because the magnetic field and polarization directions are parallel. Although the magnetic field direction is fixed, if the polarization direction was instead perpendicular to the field, an increase would be observed from the second to third region. The magnitude of the difference between regions increases and decreases with sample concentration.

RESULTS

Data collected and analyzed using method 1 is shown in Fig. 6. Graphed data is shown in Fig. 6a with the accompanying linear best fit equations and R^2 values shown in Fig. 6b. Each linear fit has an R^2 value very close to 1 as well as a y-intercept very close to 1, as expected according to theory. Using analysis described in the theory section, the values of $\Delta\sigma$ determined using method 1 are shown in Table 1. The graphed data gives three different results for $\Delta\sigma$ which are all in relevant agreement with one another.

Figure 6a.
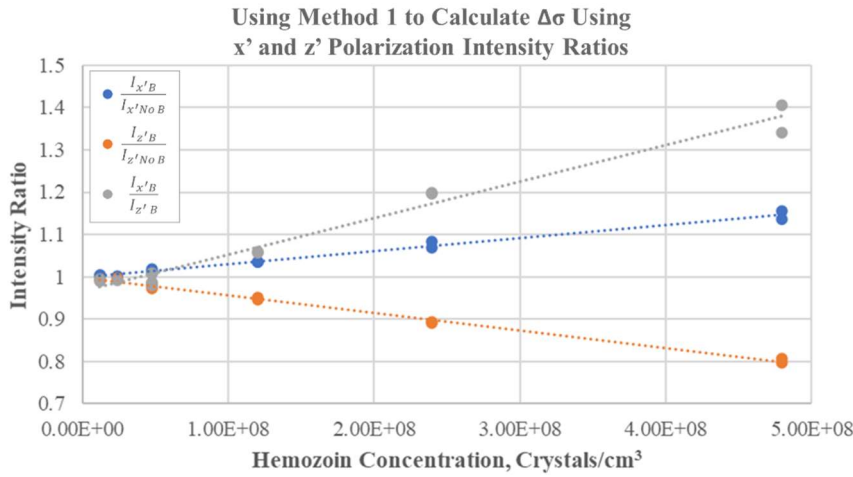
b.

$$\frac{I_{x'B}}{I_{x'No\,B}} = (3.10 \times 10^{-10} cm^3)x + 0.999$$

$$R^2 = 0.99$$

$$\frac{I_{z'B}}{I_{z'No\,B}} = (-4.16 \times 10^{-10} cm^3)x + 0.999$$

$$R^2 = 0.99$$

$$\frac{I_{x'B}}{I_{z'B}} = (8.67 \times 10^{-10} cm^3)x + 0.966$$

$$R^2 = 0.98$$

Table 1.
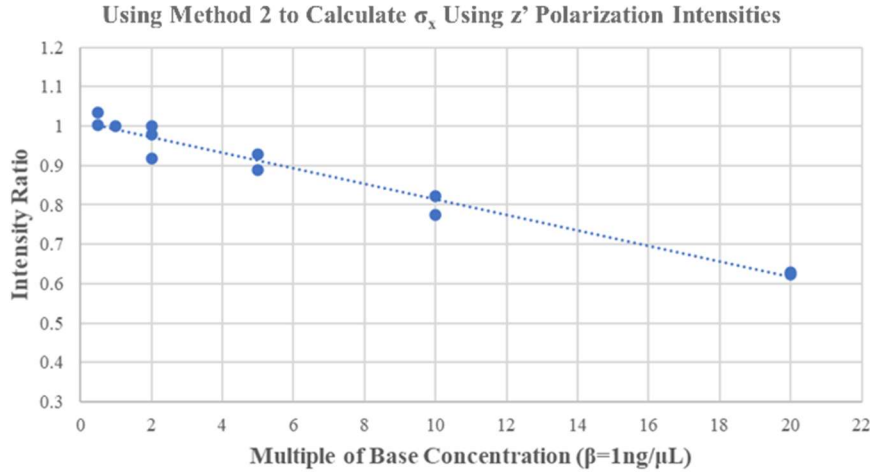
Intensity Ratio	$\Delta\sigma, cm^2$
$\dfrac{I_{x'B}}{I_{x'No\,B}}$	1.86×10^{-9}
$\dfrac{I_{z'B}}{I_{z'No\,B}}$	1.25×10^{-9}
$\dfrac{I_{x'B}}{I_{z'B}}$	1.73×10^{-9}
Average	1.61×10^{-9}

a) A graph of light intensity ratios as a function of hemozoin concentration depicting the results of method 1 with linear fits. Each dataset appears well suited to the linear fit, converging on a y-intercept of 1. **b)** The complete linear fit equations for the three intensity ratios graphed in Fig. 6a with accompanying R^2 values. **Table 1.** The $\Delta\sigma$ results for each intensity ratio in method 1 individually and an averaged final result for $\Delta\sigma$ using method 1.

Data collected and analyzed using method 2 is shown in Fig. 7. Graphed data is shown in Fig. 7a and 7c with the accompanying linear best fit equations and R^2 values shown in Fig. 7b and 7d, respectively. Again, each linear fit has an R^2 value close to 1, but slightly lesser so than in method 1. Using analysis described in the theory section, the values of $\Delta\sigma$ determined using method 2 are shown in Table 2.
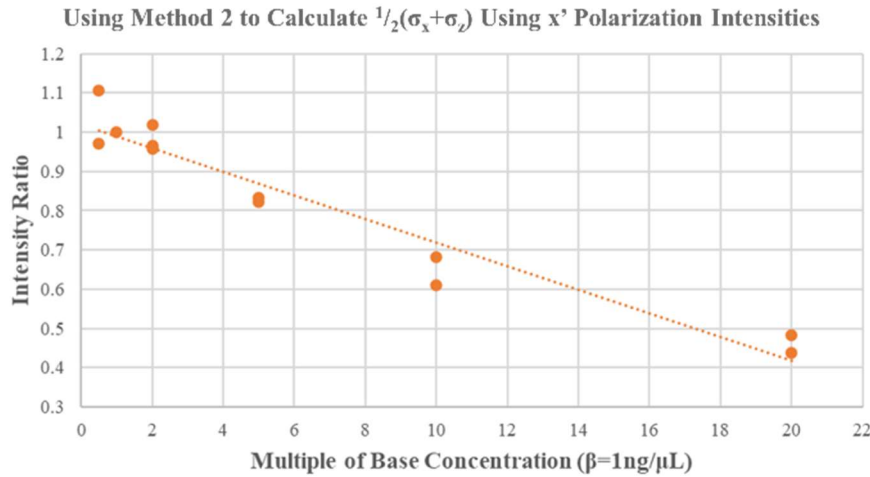
Figure 7a.

b.

$$\frac{I_{m,z'}}{I_{\beta,z'}} = -0.0239x + 1.01$$

$$R^2 = 0.97$$

Using Method 2 to Calculate σ_x Using z' Polarization Intensities

c.

d.

$$\frac{I_{m,x'}}{I_{\beta,x'}} = -0.0239x + 1.01$$

$$R^2 = 0.97$$

Using Method 2 to Calculate $\frac{1}{2}(\sigma_x+\sigma_z)$ Using x' Polarization Intensities

Table 2.

σ Term with Source	σ Term Value, cm^2
σ_x from $\frac{I_{m,z'}}{I_{\beta,z'}}$	1.25×10^{-9}
σ_z from $\frac{I_{m,x'}}{I_{\beta,x'}}$	3.99×10^{-10}
$\Delta\sigma$	8.55×10^{-10}

a) A graph of the light intensity ratio for light polarized along z' with a magnetic field applied as a function of hemozoin base concentration multiple with a linear fit which leads to an estimate of σ_x. **b)** The complete linear fit equation for the intensity ratio graphed in Fig. 7a with an accompanying R^2 value. **c)** A graph of the light intensity ratio for light polarized along x' with a magnetic field applied as a function of hemozoin base concentration multiple with a linear fit which leads to an estimate of σ_z. **d)** The complete linear fit equation for the intensity ratio graphed in Fig. 7c with an accompanying R^2 value. **Table 2.** The individual σ terms derived using method 2 and the $\Delta\sigma$ term those results produce.

To check method 2's result for $\Delta\sigma$, Eq. (19) is graphed in Fig. 8a for light polarized along the x' and z' axes with accompanying linear best fit equations and R^2 values shown in Fig. 8b. Using analysis from the theory section, a σ term can be extracted from each slope and compared to the same term calculated using results for σ from method 2. The three results are shown in Table 3 and the agreement of the results, provides assurance that the theory underlying method 2 is sound.

Figure 8a.

Using Method 2 to Calculate $^2/_3\sigma_x + ^1/_3\,\sigma_z$
Using x' and z' Polarization Intensities

Legend:
- $\dfrac{I_{m,x'\,No\,B}}{I_{\beta,x'\,No\,B}}$
- $\dfrac{I_{m,z'\,No\,B}}{I_{\beta,z'\,No\,B}}$

Y-axis: Intensity Ratio
X-axis: Multiple of Base Concentration (β=1ng/μL)
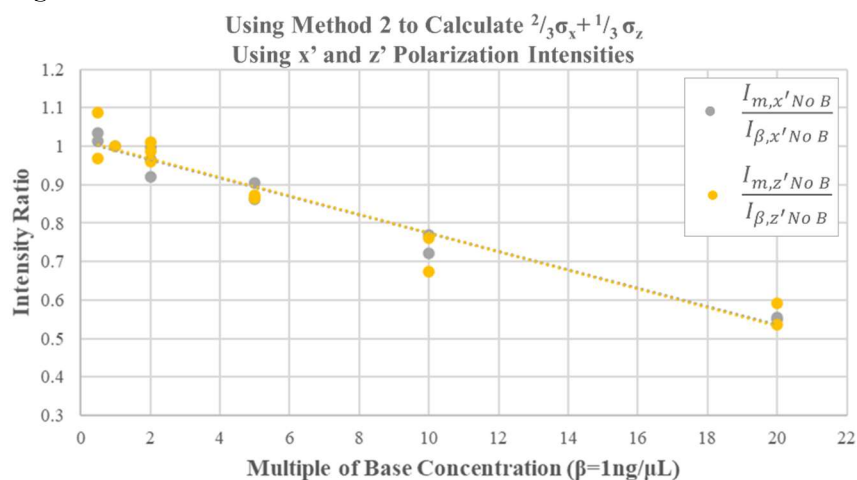
b.

$$\frac{I_{m,x'\,No\,B}}{I_{\beta,x'\,No\,B}} = -0.0239x + 1.01$$

$$R^2 = 0.97$$

$$\frac{I_{m,z'\,No\,B}}{I_{\beta,z'\,No\,B}} = -0.0242x + 1.02$$

$$R^2 = 0.93$$

Table 3.

Source of σ Term Calculation	$\dfrac{2}{3}\sigma_x + \dfrac{1}{3}\sigma_z$ Estimate, cm^2
$\dfrac{I_{m,x'\,No\,B}}{I_{\beta,x'\,No\,B}}$	9.95×10^{-10}
$\dfrac{I_{m,z'\,No\,B}}{I_{\beta,z'\,No\,B}}$	1.01×10^{-9}
Method 2 Estimate of σ_x and σ_z	9.69×10^{-10}

a) A graph of light intensity ratios for light polarized along x' and z' without a magnetic field applied as a function of hemozoin base concentration multiple with a linear fit which leads to an estimate of $\frac{2}{3}\sigma_x + \frac{1}{3}\sigma_z$. Although, two linear fits are shown, as expected, the fits are nearly identical and are difficult to distinguish on the graph. **b)** The complete linear fit equations for the intensity ratios graphed in Fig. 8a with accompanying R^2 values. **Table 3.** A comparison of the $\frac{2}{3}\sigma_x + \frac{1}{3}\sigma_z$ terms from both fits alongside with the same term calculated using the σ values from method 2.

The $\Delta\sigma$ results from both methods are compared in Table 4, demonstrating that both methods arrive at a similar result for $\Delta\sigma$ of hemozoin crystals. The consistency observed gives further evidence in support of the theory underlying the calculations, subsequently lending support to the final result for $\Delta\sigma$, $(1.4 \pm 0.4) \times 10^{-9} cm^2$, as well.

Table 4.

Source for $\Delta\sigma$ Estimate	$\Delta\sigma, cm^2$
Method 1	1.61×10^{-9}
Method 2	8.55×10^{-10}
Average of Methods	$(1.4 \pm 0.4) \times 10^{-9}$

A comparison of the final $\Delta\sigma$ results from method 1 and 2 as well as an average of the three estimates from method 1 and a fourth estimate from method 2 which gives a final result for $\Delta\sigma$ plus or minus a standard deviation.

DISCUSSION

Comparison of $\Delta\sigma$ from each method provides a more accurate assessment of the true $\Delta\sigma$ for hemozoin crystals. The results from both methods are in relative agreement with one another though there is a significant standard

deviation associated with the final result for $\Delta\sigma$. The similarity to other optical properties of hemozoin numerically related to absorption cross section published by Butykai, et al. supports the reported result for $\Delta\sigma$ though.[6]

The discrepancy in the final result still warrants discussion. The large standard deviation is likely a result of one of two possible sources of experimental error. The laser used with the MOD had potential issues because of the laser's shape. Looking back to Table 1, $\Delta\sigma$ calculated from light polarized in the z' direction was consistently lower than the other ratios used in method 1. This might be attributable to the width of the beam being too large and it subsequently interacting with the cuvette during transmission or potentially to the cuvettes acting as polarizers.

Another source of error is in the accuracy of the concentrations of each hemozoin sample tested. This arose from a combination of human errors as well as limitations of the equipment used. Additionally, older samples tended to lose some volume of PBS while in storage due to evaporation which could have disproportionately and indiscriminately changed the concentration of samples. Any repeatability studies carried out with hemozoin would require further investigation and elimination of these errors and other potential errors to ensure an accurate measurement of $\Delta\sigma$.

CONCLUSION

The success of the MOD in industry as well as the positive results produced by this research demonstrate the diagnostic capabilities of the MOD. This is true of malaria and hemozoin, but this success informs and improves ongoing research into MOD's ability to detect other hemozoin-like crystals. Beyond these physically unique crystals, this research also informs the use of MOD in broader diagnostic endeavors using magnetic nanoparticles. With a solid physical understanding of the detection mechanism used for hemozoin, the MOD is well positioned to expand its applications in the future.

AKNOWLEDGEMENTS

REFERENCES

1. World Health Organization, World Malaria Report 2019, (2019).

2. P. White, "Hemex Health licenses breakthrough medical technologies focused on preventing hundreds of thousands of deaths annually" (in press, 2016).

3. L. M. Coronado, C. T. Nadovich, and C. Spadafora, Biochim Biophys Acta. **1840**, 2032 (2014).

4. M. Olivier, K. Van Den Ham, M. T. Shio, F. A. Kassa, and S. Fougeray, Front Immunol. **5**, 25 (2014).

5. R. H. Pek, X. Yuan, N. Rietzschel, J. Zhang, L. Jackson, E. Nishibori, A. Ribeiro, and W. Simmons, eLife **8**, e49503 (2019).

6. A. Butykai, A. Orban, V. Kocsis, D. Szaller, S. Bordacs, E. Tatrai-Szekeres, L.F. Kiss, A. Bota, B.G. Vertessy, T. Zelles, and I. Kezsmarki, Nature **3**, 1431 (2013).

7. E. Hecht and A. R. Ganesan, in *Optics* (Pearson, Noida, India, 2008).

8. D. Kara (private communication, June 3, 2019).

9. J. L. Jimenez, "Spectroscopy and photochemistry II" (lecture, 2005).

10. B. T. Grimberg, R. Deissler, W. Condit, R. Brown, J. Jones, and R. Bihary, US patent 977245 B2 (2017).

11. D. Kara (private communication, March 12, 2020).

12. D. Kara (private communication, April 10, 2020).

APPENDIX

Intensity data measured in the laboratory and used in Beer's law is useful in pursuit of $\Delta\sigma$, but it is important that the result relate to the correct frame of reference. Data is collected in the laboratory frame which contributes to results for $\sigma_{x'}$ and $\sigma_{z'}$, however, $\Delta\sigma$ is sought in relation to the crystal frame of reference. To unite the two coordinate systems, a basis transformation and averaging over many crystal orientations must be done.

The transformation of bases starts with another physical property related to σ though, the electric dipole moment. The electric diploe moment of a material, $\vec{p}$, can be related to an external electric field, $\vec{E}$, by a polarizability tensor, $\overleftrightarrow{\alpha}$.

$$\vec{p} = \overleftrightarrow{\alpha}\,\vec{E} \tag{1A}$$

This polarizability tensor is, in turn, related to the absorption cross section as in Eq. (2A), where σ_ϵ is the absorption cross section for light polarized in the ϵ direction, $\alpha_{\epsilon\epsilon}$ is the $\epsilon\epsilon$ component of the polarizability tensor $\vec{\alpha}$, and k is a constant.

$$\sigma_\epsilon = k \, Im\{\alpha_{\epsilon\epsilon}\} \tag{2A}$$

In the crystal frame of reference, the polarizability tensor is diagonal.

$$\vec{\alpha} = \begin{bmatrix} \alpha_{xx} & 0 & 0 \\ 0 & \alpha_{yy} & 0 \\ 0 & 0 & \alpha_{zz} \end{bmatrix} \tag{3A}$$

Given the symmetry of hemozoin's easy plane shown in Fig. 2a, it is expected that the xx and yy components of the polarizability tensor would be equal.

$$\alpha_{xx} = \alpha_{yy} \tag{4A}$$

Additionally, considering hemozoin's dichroic nature, it is also expected that the xx component of the tensor will be greater than the zz component.

$$\alpha_{xx} > \alpha_{zz} \tag{5A}$$

When measuring crystals' absorption cross section in solution in the laboratory frame though, the measured values are an average over many possible crystal orientations related to the polarizability tensor in the laboratory frame, $\vec{\alpha}'$.

$$\vec{\alpha}' = \begin{bmatrix} \alpha_{x'x'} & \alpha_{x'y'} & \alpha_{x'z'} \\ \alpha_{y'x'} & \alpha_{y'y'} & \alpha_{y'z'} \\ \alpha_{z'x'} & \alpha_{z'y'} & \alpha_{z'z'} \end{bmatrix} \tag{6A}$$

If light is polarized in the x' direction then, an average for $\sigma_{x'}$, $\langle\sigma_{x'}\rangle$, is measured.

$$\langle\sigma_{x'}\rangle = k \, Im\{\langle\alpha_{x'x'}\rangle\} \tag{7A}$$

A similar result is given for light polarized in the z' direction.

$$\langle\sigma_{z'}\rangle = k \, Im\{\langle\alpha_{z'z'}\rangle\} \tag{8A}$$

Here, the averages are taken over random θ when no magnetic field is applied (measured from the z axis) and random ϕ (measured from the x axis).

$$\langle f(\theta)\rangle_\theta = \frac{1}{2}\int_0^\pi f(\theta) \sin\theta \, d\theta \tag{9A}$$

$$\langle f(\phi)\rangle_\phi = \frac{1}{2\pi}\int_0^{2\pi} f(\phi) \, d\phi \tag{10A}$$

To relate measured values of $\sigma_{\epsilon\epsilon}$ to the crystal frame that is desired, $\vec{\alpha}$ and $\vec{\alpha}'$ need to be related using a basis transformation. This basis transformation needs to be applied as in Eq. (11A), where Q is a transformation matrix.

$$\vec{\alpha}' = Q \, \vec{\alpha} \, Q^{-1} \tag{11A}$$

Euler angles can be used to find Q, but in this transformation, only two rotations are required. The first rotation is by an angle, θ, about the x axis. Note that when the magnetic field is applied to the sample, $\theta = 90°$ because the z and z' axes are perpendicular to one another, but when the magnetic field is not applied, θ is random because the position of the z axis relative to the z' axis is random.

$$R_x(\theta) = \begin{bmatrix} 1 & 0 & 0 \\ 0 & \cos\theta & \sin\theta \\ 0 & -\sin\theta & \cos\theta \end{bmatrix} \tag{12A}$$

The second rotation matrix, $R_z(\phi)$, allows for random orientation of the easy plane parallel to the magnetic field.

$$R_z(\phi) = \begin{bmatrix} \cos\phi & \sin\phi & 0 \\ -\sin\phi & \cos\phi & 0 \\ 0 & 0 & 1 \end{bmatrix} \tag{13A}$$

Together, Eqs. (12A) and (13A) define Q.

$$Q = R_z(\phi) \, R_x(\theta) \tag{14A}$$

Using this transformation, the polarizability tensor in the laboratory frame can be translated to the crystal frame. This gives Eqs. (15A), (16A), and (17A). In the case of $\langle \alpha_{x'x'} \rangle$ and $\langle \alpha_{z'z'} \rangle$, $\theta = 90°$ and in the case of $\langle \alpha_{No\,B} \rangle$, θ is random as was previously mentioned.

$$\langle \alpha_{x'x'} \rangle = \frac{1}{2}\alpha_{xx} + \frac{1}{2}\alpha_{zz} \tag{15A}$$

$$\langle \alpha_{z'z'} \rangle = \alpha_{xx} \tag{16A}$$

$$\langle \alpha_{No\,B} \rangle = \frac{2}{3}\alpha_{xx} + \frac{1}{3}\alpha_{zz} \tag{17A}$$

Given the relationship between the polarizability tensor and the absorption cross section, the translation of α from one basis to another can be readily applied to σ, completing the derivation of Eqs. (3), (4), and (5).[11,12]

$$\langle \sigma_{x'B} \rangle = \frac{1}{2}\sigma_x + \frac{1}{2}\sigma_z \tag{3}$$

$$\langle \sigma_{z'B} \rangle = \sigma_x \tag{4}$$

$$\langle \sigma_{No\,B} \rangle = \frac{2}{3}\sigma_x + \frac{1}{3}\sigma_z \tag{5}$$